Broadband all-electronically tunable MEMS terahertz quantum cascade lasers

Ningren Han,[1,*] Alexander de Geofroy,[2] David P. Burghoff,[1] Chun Wang I. Chan,[1] Alan Wei Min Lee,[2] John L. Reno,[3] and Qing Hu[1]

[1]*Department of Electrical Engineering and Computer Science, Massachusetts Institute of Technology, Cambridge, Massachusetts 02139, USA*

[2]*LongWave Photonics LLC, Mountain View, California 94043, USA*

[3]*Center for Integrated Nanotechnologies, Sandia National Laboratories, Albuquerque, New Mexico 87123, USA*

**Corresponding author: ningren@mit.edu*

Received April 28, 2014; accepted May 7, 2014;
posted May 9, 2014 (Doc. ID 210950); published June 5, 2014

In this work, we demonstrate all-electronically tunable terahertz quantum cascade lasers (THz QCLs) with MEMS tuner structures. A two-stage MEMS tuner device is fabricated by a commercial open-foundry process performed by the company MEMSCAP. This provides an inexpensive, rapid, and reliable approach for MEMS tuner fabrication for THz QCLs with a high-precision alignment scheme. In order to electronically actuate the MEMS tuner device, an open-loop cryogenic piezo nanopositioning stage is integrated with the device chip. Our experimental result shows that at least 240 GHz of single-mode continuous electronic tuning can be achieved in cryogenic environments (~4 K) without mode hopping. This provides an important step toward realizing turn-key bench-top tunable THz coherent sources for spectroscopic and coherent tomography applications. © 2014 Optical Society of America

OCIS codes: (140.3070) Infrared and far-infrared lasers; (230.4685) Optical microelectromechanical devices.
http://dx.doi.org/10.1364/OL.39.003480

Terahertz quantum cascade lasers (THz QCLs) are promising solid-state sources of coherent THz radiation [1,2]. High power [3], high maximum operating temperature [4], broad tunability [5,6], good beam pattern [7,8], and frequency comb formation [9] together with their inherent compactness and reliability make THz QCLs extremely competitive when compared with other coherent THz sources that are currently available. Single-mode, continuous tunability over a broad bandwidth is especially important for applications such as broadband THz spectroscopy [10] and THz coherent tomography [11].

Recently, intracavity difference-frequency generation in dual-wavelength mid-infrared quantum cascade lasers has shown impressive tuning capacity as a way to achieve tunable THz laser source [12]. The large power dissipation due to the nonlinear optical process makes continuous-wave (CW) operation difficult without significant engineering on thermal management. As an alternative, the concept of a so-called "THz wire laser" can be used to realize robust broadband THz tunability [5,6]. By manipulating the near-field transverse mode profile around the ridge of a THz wire laser using an external object, known as a tuner, one can effectively change the transverse component of k of the resonant mode. Meanwhile, the small active region area is advantageous for CW performance compatible with existing miniature cryocooler-based platforms [11], making tunable THz wire lasers especially suitable for applications requiring CW operation such as local oscillators in heterodyne receivers.

Although this mechanism exhibits unprecedented tuning performance for THz QCLs [13], the MEMS tuner device was previously actuated by the manual turning of a differential micrometer fed through the wall of a cryostat. In addition to the large thermal load introduced by the micrometer, the manual tuning scheme requires extremely careful operation and is not suitable for general users. Therefore, an all-electronically driven actuator that is able to work at cryogenic temperatures is needed to replace the manual tuning scheme. In addition, the previously developed in-house MEMS tuner chip fabrication requires many photolithography and etching steps [14]. This high-processing complexity and long iteration cycle could be greatly alleviated by leveraging standard customized MEMS foundry processes for the tuner fabrication. Here we demonstrate that the commercial MEMS foundry platform SOIMUMPs from the company MEMSCAP can be integrated with the tunable THz QCL scheme using careful design [15]. The electronic tuner actuation is achieved with an open-loop cryogenic piezo nanopositioning stage (PI miCos Piezo Positioner PP-17). By combining these two elements with the tunable THz wire laser, all electronic tunability is achieved with a compact device footprint.

The SOIMUMPs platform allows patterning and etching down to the buried oxide layer from the device and handle sides of an SOI wafer. In addition to these two silicon processing steps, two patterned metal deposition processes are embedded in the platform as well. Since the alignment between the THz QCL chip and the MEMS tuner chip is crucial for the tuning performance, a flip-chip alignment scheme is employed as opposed to the previous through-hole alignment technique [14]. For the QCL design, first-order DFB wire lasers with sinusoidal corrugations on one side are physically connected to the bonding pad through finger-like mode selectors in order to improve the mode selectivity as shown in Fig. 1(a) [16]. The average width of the wire laser is around 10 μm to ensure a wide tuning range and also to avoid any higher-order lateral modes from lasing. The target resonator frequency is designed by adjusting the corrugation periodicity with finite-element method (FEM) simulations in COMSOL. Female alignment structures are patterned and etched from the same photolithography and dry etch processes used to define the laser structure. All the surface structures on the QCL chip are of 10 μm height. An SEM image showing the fabricated wire laser device is shown in Fig. 1(b).

 © 2014 Optical Society of America

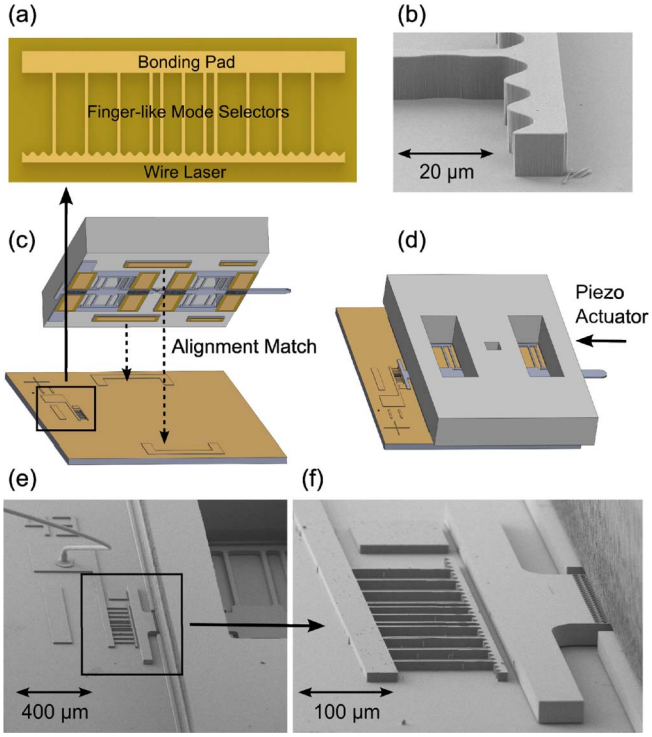

Fig. 1. (a) Top view of the wire laser connected to the bonding pad through finger-like mode selectors. (b) SEM image showing the fabricated THz wire laser with first-order sinusoidal corrugations on one side. (c) and (d) Alignment illustration for the tuner and QCL chips. (e) and (f) SEM images showing the alignment between the tuner and the QCL chip, which indicate no visual misalignment. The tuner object is suspended around 1 to 2 μm above the QCL chip bottom surface as designed.

The MEMS tuner device employs a two-stage folded-beam flexure design. When pushed by an external object, the first-stage flexure mitigates the effect of any tilted force exertion on the actuation shaft, thereby minimizing any lateral torque applied on the second-stage flexure. Apart from the flexure structure, the male alignment features are defined on the same silicon layer. Since all critical features on the silicon device layer are patterned in the same photolithography step, feature misalignment due to inter-lithography mask misalignment is minimized. This is crucial to obtain highly repeatable and reproducible tuning result, since even a few micrometers of misalignment between the wire laser and the tuner could significantly reduce the tuning range [14]. The top silicon structure layer thickness on the MEMS tuner chip is 25 μm for all the devices tested, which sets the height for the tuner surface. With the flip-chip alignment scheme depicted in Figs. 1(c) and 1(d), it is important to ensure that the folded-beam flexure structure is not stuck in between the tuner chip and the QCL chip during actuation. Such design consideration is taken care of by utilizing the two metal deposition processes in the SOIMUMPs, which deposit in total of around 1.2 μm thick metal on top of the selected silicon area. This ~1.2 μm thick buffer layer, shown in Figs. 2(b) and 2(c), will keep the tuner flexure structure elevated from the QCL chip surface during actuation while maintaining large vertical overlap between the wire laser ridge and the tuner surface.

Standard wafer dicing is carried out to separate individual MEMS tuner chips on the 1.1 cm × 1.1 cm die site from the SOIMUMPs. As illustrated in Figs. 2(a) and 2(b), in regions of the extended tuner object or the actuation shaft, the through-hole trench is intentionally widened in the lateral direction. When the wafer dicing saw tool cuts along the mark shown in the figure, the excessive region in front of either the tuner object or the actuation shaft will fall-off the chip automatically, leaving the tuner object and the actuation shaft extending out of the device chip. A metal sputtering process is carried out to coat the side wall of the tuner surface with gold as tuning with metal tuners in general exhibits higher range compared with silicon tuners [6]. Two SEM images showing the two-stage folded-beam flexure tuner chip are shown in Figs. 2(d) and 2(e).

Standalone THz wire laser testing without the tuner chip attachment is first carried out to determine the lasing performance. The characterization plots for a wire laser with an 11-finger enhanced mode selector design at liquid helium temperature are shown in Fig. 3. The laser bias is pulsed with a repetition rate of 20 kHz and a pulse duration of 500 ns (1% duty cycle). The wire laser tested has an average width of 9.5 μm, a corrugation periodicity of 15.2 μm, and a total corrugation number of 30. This results in a total laser length of 456 μm. The design frequency is at 3.72 THz and is calculated assuming that the refractive index of the active region is 3.6. The simulated cavity mode threshold gain plot of the wire laser is shown in the right inset of Fig. 3. The lasing spectra measured using a Fourier transform infrared spectroscopy (FTIR) across different biasing

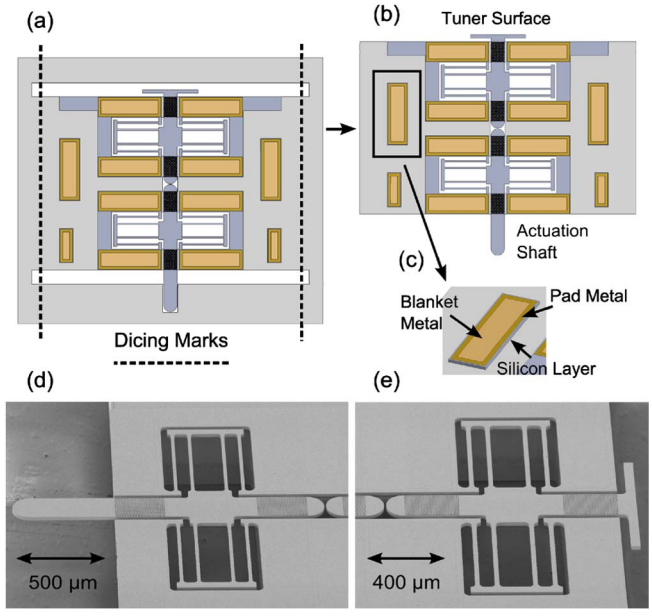

Fig. 2. (a) and (b) Top view schematics showing the dicing marks along which a wafer-dicing saw tool is used for chip separation and finishing. (c) Closer look at the alignment feature on the tuner chip, which shows the two metal layers deposited within the SOIMUMPs platform. The metal layers serve as the ~1.2 μm thick buffer layer in between the tuner and QCL chip. (d) and (e) SEM images showing the two-stage folded-beam flexure tuner chip fabricated from the SOIMUMPs platform.

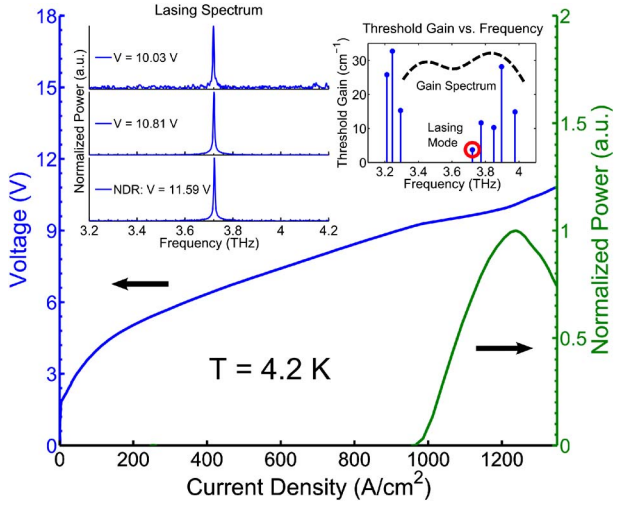

Fig. 3. Performance characterization plots for a standalone THz wire laser chip in pulsed operation (1% duty cycle). The V-J and L-J curves are both measured at liquid helium temperature of around 4.2 K. The left inset shows the lasing spectra measured with FTIR across different bias points. This wire laser lases at around 3.72 THz without the presence of the MEMS tuner chip. The right inset shows the simulated cavity mode threshold gain plot. The mode encircled in red is the designed lasing mode. The dotted curve indicates the estimated gain spectrum.

voltages are shown in the left inset of Fig. 3, which show that the bare wire laser operates at a frequency of 3.72 THz. The maximum lasing temperature T_{max} for this laser is around 100 K, whereas a standard 40 μm wide Fabry–Perot laser from the same gain medium has a T_{max} of around 166 K. An accurate account for the absolute power is difficult to obtain due to the lack of a suitable power meter for the small power collected from the wire laser. An estimation based on the photodetector voltage reading indicates a collected power on the order of ~tens of μW for typical wire laser devices.

In order to show that wire lasers are suitable for CW operation, the performance of a device under CW operation and under pulsed operation is plotted in Fig. 4. The laser is biased at a repetition rate of 20 kHz in the pulsed mode with duty cycles of 1% and 10% and also in the CW mode inside a pulse tube cryocooler, which maintains the

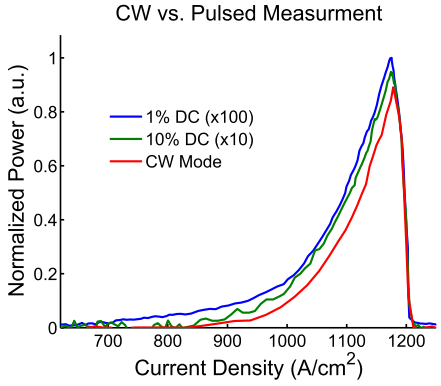

Fig. 4. L-J plots for a THz wire laser under CW operation and pulsed operation at 35 K. The light outputs at different duty cycles (DCs) are scaled by the ratio of the corresponding DC compared to 100% (CW mode).

device temperature at 35 K. The performance at different duty cycles can be compared by scaling the pulsed laser's light output by the ratio of the duty cycles (i.e., by 10 or 100). The results show comparable device performance between CW and pulsed operations, with the peak power dropping by about 5% when going from 1% to 10% duty cycle, and another 5% when going from 10% to 100% (CW) duty cycle. This comparable CW and pulsed performance is expected from such a narrow device in which heat removal is easily manageable.

After the standalone QCL characterization, the tuner chip, separated from the SOIMUMPs device die, is backflipped and microaligned with the QCL chip as illustrated in Figs. 1(c) and 1(d). Two SEM images showing the tuner chip bonded with the QCL chip are shown in Figs. 1(e) and 1(f). The pictures demonstrate that the tuner chip is well aligned with the QCL chip. The side view in Fig. 1(f) shows that the tuner object is suspended around 1 to 2 μm above the QCL chip surface as designed with the buffer of the double metal layer.

The assembled device is then attached to a device mount as illustrated in Fig. 5(a). The extruded actuation shaft is pushed by the copper arm attached to the piezo nanopositioning actuator. Devices are tested and characterized inside a cryogenic dewar at liquid helium temperature in 1% pulsed operation. The low duty cycle is chosen to prolong the holding time of liquid helium, while still maintaining adequate signal-to-noise ratio. The piezo nanopositioning actuator has an open-loop actuation precision of about a few nanometers. Almost all the

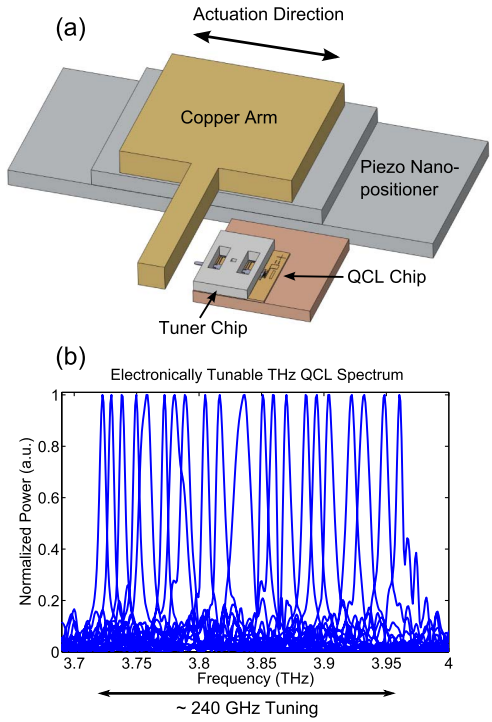

Fig. 5. (a) Schematic illustration showing the mounted device with the piezo nano-positioning actuator. A copper arm is attached to the piezo actuator in order to physically contact the tuner actuation shaft during the tuning process. (b) Normalized spectrum for the electronically tunable THz QCL characterized in Fig. 3. The tuning starts from 3.72 THz and ends at 3.96 THz with a range of 240 GHz with single-mode continuous tuning behavior.

devices tested demonstrate over 200 GHz single-mode continuous tuning performance, showing the repeatability and robustness of the alignment scheme. The normalized tuning spectrum for the device characterized in Fig. 3 is shown in Fig. 5(b). By moving the piezo nanopositioning actuator with the control program, the lasing frequency is altered in a reversible manner. The coverage of the lasing spectrum spans across 3.72 to 3.96 THz, giving a tuning range of 240 GHz. No mode hopping or multimode lasing is observed, which shows the efficacy of wire lasers with enhanced mode selectors. Beyond 3.96 THz, no active signal can be detected with the FTIR measurement, likely because of a strong water-absorption feature covering 3.95 to 4.00 THz that cannot be completely removed by nitrogen purging. When the tuner is moved closer to the laser than the 3.96 THz position (that is, when attempting to tune to higher than 3.96 THz), a signal can nonetheless still be detected when the photodetector is placed directly adjacent to the laser dewar. This confirms the hypothesis of water absorption. This signal gradually decreases to zero when moving the tuner further, most likely due to the fast roll-off of the gain spectrum when reaching the edge of the gain bandwidth. Although only pulsed tuning operation is shown here, based on the CW measurement of the standalone device, one could expect similar CW tuning performance. The tunable laser device footprint is compact, and it only requires two additional electrical ports for the actuator as compared with standalone QCL device operation. This eases system-level integration with compact cryogenic coolers.

In summary, this work improves the previous manually tunable THz QCLs by adding turn-key electronic tunability. By leveraging the commercial foundry platform SOIMUMPs, a robust, reproducible, and cost-effective solution for integrating electronically actuated MEMS tuner chips with THz wire laser chips is demonstrated. Such implementation greatly reduces the cost and iteration time for producing electronically tunable THz lasers. Future work includes improving the power performance and beam pattern using THz power amplifiers as well as integration with compact cryogenic coolers to enable CW turn-key tuning.

The work at MIT is supported by NASA, NSF and the Siebel Foundation. The work at Sandia is performed, in part, at the Center for Integrated Nanotechnologies, a U.S. Department of Energy Office of Basic Energy Sciences user facility. Sandia National Laboratories is a multiprogram laboratory managed and operated by Sandia Corporation, a wholly owned subsidiary of Lockheed Martin Corporation, for the U.S. Department of Energy's National Nuclear Security Administration under contract DE-AC04-94AL85000. The author would like to acknowledge Qi Qin and Tsung-Yu Kao for their help in experimental design and device fabrication.

References

1. R. Köhler, A. Tredicucci, F. Beltram, H. E. Beere, E. H. Linfield, A. G. Davies, D. A. Ritchie, R. C. Iotti, and F. Rossi, Nature **417**, 156 (2002).
2. B. S. Williams, Nat. Photonics **1**, 517 (2007).
3. M. Brandstetter, C. Deutsch, M. Krall, H. Detz, D. C. MacFarland, T. Zederbauer, A. M. Andrews, W. Schrenk, G. Strasser, and K. Unterrainer, Appl. Phys. Lett. **103**, 171113 (2013).
4. S. Fathololoumi, E. Dupont, C. W. I. Chan, Z. R. Wasilewski, S. R. Laframboise, D. Ban, A. Mátyás, C. Jirauschek, Q. Hu, and H. C. Liu, Opt. Express **20**, 3866 (2012).
5. Q. Qin, B. S. Williams, S. Kumar, J. L. Reno, and Q. Hu, Nat. Photonics **3**, 732 (2009).
6. Q. Qin, J. L. Reno, and Q. Hu, Opt. Lett. **36**, 692 (2011).
7. M. I. Amanti, M. Fischer, G. Scalari, M. Beck, and J. Faist, Nat. Photonics **3**, 586 (2009).
8. T.-Y. Kao, Q. Hu, and J. L. Reno, Opt. Lett. **37**, 2070 (2012).
9. D. Burghoff, T.-Y. Kao, N. Han, I. C. W. Chan, X. Cai, Y. Yang, D. J. Hayton, J. R. Gao, J. L. Reno, and Q. Hu, Nat. Photonics **8**, doi: 10.1038/nphoton.2014.85 (2014).
10. B. Ferguson and X.-C. Zhang, Nat. Mater. **1**, 26 (2002).
11. A. Wei Min Lee, T.-Y. Kao, D. Burghoff, Q. Hu, and J. L. Reno, Opt. Lett. **37**, 217 (2012).
12. K. Vijayraghavan, Y. Jiang, M. Jang, A. Jiang, K. Choutagunta, A. Vizbaras, F. Demmerle, G. Boehm, M. C. Amann, and M. A. Belkin, Nat. Commun. **4**, 2021 (2013).
13. M. S. Vitiello and A. Tredicucci, IEEE Trans. Terahertz Sci. Technol. **1**, 76 (2011).
14. Q. Qin and Q. Hu, J. Micromech. Microeng. **21**, 075004 (2011).
15. A. Cowen, G. Hames, D. Monk, S. Wilcenski, and B. Hardy, *SOIMUMPs Design Handbook*, (MEMSCAP Inc., 2011), Revision 8.0.
16. Q. Qin, N. Han, T. Kao, J. L. Reno, and Q. Hu, Opt. Lett. **38**, 407 (2013).